Electronic Supplementary Material (ESI) for Journal of Materials Chemistry C.
This journal is © The Royal Society of Chemistry 2021

# Supporting Information

*Yingfeng Ruan, Pengju Guo, Zhiping Zheng*, Qiuyun Fu*, Rongda Zhou, Hualin Chen, Geng Wang, Wei Luo*

School of Optical and Electronic Information, Engineering Research Center for Functional Ceramics of the Ministry of Education, Huazhong University of Science and Technology, Wuhan 430074, P. R. China

Full affiliation address: No. 1037, Luoyu Road, Hongshan District, Wuhan, Hubei Province, P. R. China, 430074

**Corresponding Author**

*Email: zzp@mail.hust.edu.cn; Phone**: +86-27-87545167.**

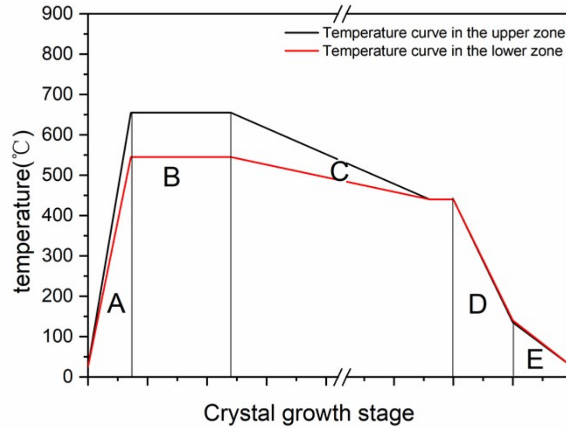


**Figure S1.** Schematic diagram of crystal growth stages

**Fabrication of the $CsPbBr_3$.** The furnace was first heated up to the melting point of $CsPbBr_3$ polycrystalline powders and held for a few hours. Then the furnace started cooling down for crystal growth. The temperature gradient during this stage is 10 °C/cm and the growth rate of $CsPbBr_3$ crystal is 0.5 mm/h. The cooling process was conducted at a rate of 10 °C/h, while the cooling process proceeded at a smaller cooling rate of 1 °C/h when reached 130 °C and 88 °C, which are phase transformation point. Finally, the temperature of the furnace decreased to room temperature in few hours to finish the crystal growth of $CsPbBr_3$.

The crystal was cut into wafers with a thickness of 2 mm by a wire cutting machine. Then we polished the surfaces of the wafers with $Al_2O_3$ abrasives in diameter of 14 μm, 7 μm, 1.5 μm and 0.5 μm. These polished $CsPbBr_3$ wafers were immersed in absolute ethyl alcohol to remove abrasives and other impurities.

**Material characterization.** The crystal structure and phase purity of $CsPbBr_3$ crystal were identified by X-ray diffraction equipment (XRD, X'Pert PRO Systems, PANa-lytical B.V., Netherlands). The the UV-vis transmittance spectra of the wafer was tested by Perkin-Elmer Lambda 35 ultraviolet spectrophotometer(wavelength range 190-900 nm) at room temperature.

Current-voltage curves for photoconductivity and leakage current were measured using Agilent B1500A analyzer.

**Detector performance measurement.** For X-ray detector performance, a tungsten anode X-ray tube (HAMAMATSU L9421-02) was used as the source. The X-ray source was operated with a constant 50 kV acceleration.voltage. A 2 mm-thick Al foil was inserted between the source and $CsPbBr_3$ X-ray detectors to serve as the attenuator to filter the low-energy X-rays. The dose rate was changed by changing the X-ray tube current. A Keithley 2635 Source Meter was used to apply the bias voltage and record the response current. All measurements were taken at room temperature in air.

**Table S1.** Measurements of Hall Effect at 300 K for the $CsPbBr_3$ crystal.

| | Bulk concentration ($cm^{-3}$) | Sheet concentration ($cm^{-3}$) | Resistivity($\Omega \cdot cm$) | Average hall coefficient($m^3/C$) |
|---|---|---|---|---|
| 1 | $-2.532 \times 10^{11}$ | $-1.306 \times 10^{10}$ | $1.125 \times 10^{8}$ | $-2.466 \times 10^{7}$ |
| 2 | $-2.563 \times 10^{11}$ | $-1.322 \times 10^{10}$ | $2.844 \times 10^{6}$ | $-2.436 \times 10^{7}$ |
| 3 | $-2.734 \times 10^{11}$ | $-1.411 \times 10^{10}$ | $4.710 \times 10^{6}$ | $-2.283 \times 10^{7}$ |

**Table S2.** The X-ray dose rate under different accelerating current.

| Current(μA) | 140 | 120 | 100 | 80 | 60 | 40 | 20 |
|---|---|---|---|---|---|---|---|
| Dose rate ($mGy_{air}s^{-1}$) | 5.50 | 4.71 | 3.93 | 3.14 | 2.36 | 1.57 | 0.79 |

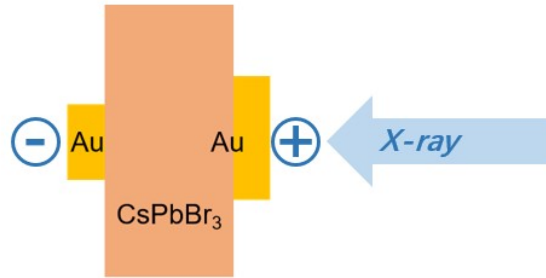


**Figure S2.** Schematic diagram of X-ray response, the direction of X-ray

We calculated the electric field inside devices: Au(1)/$CsPbBr_3$/Au(4), Au(1.5)/$CsPbBr_3$/Au(4), Au(3)/$CsPbBr_3$/Au(4), Au(4)/$CsPbBr_3$/Au(4), and got these electric-field intensity-distribution cloud maps. The electric field distribution inside the device calculated by Ansys software is basically the same as the above speculated core-like model. When the diameter ratio of the upper and lower electrodes is m : n (m < n), the electric field inside the material presents a conical distribution. As the upper electrode diameter increases until it equals the lower one, the electric field distribution inside the wafer gradually becomes symmetrical.

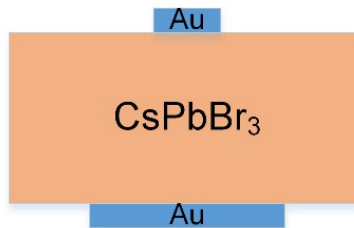


**Figure S3.** The calculation model of Finite Element Analysis

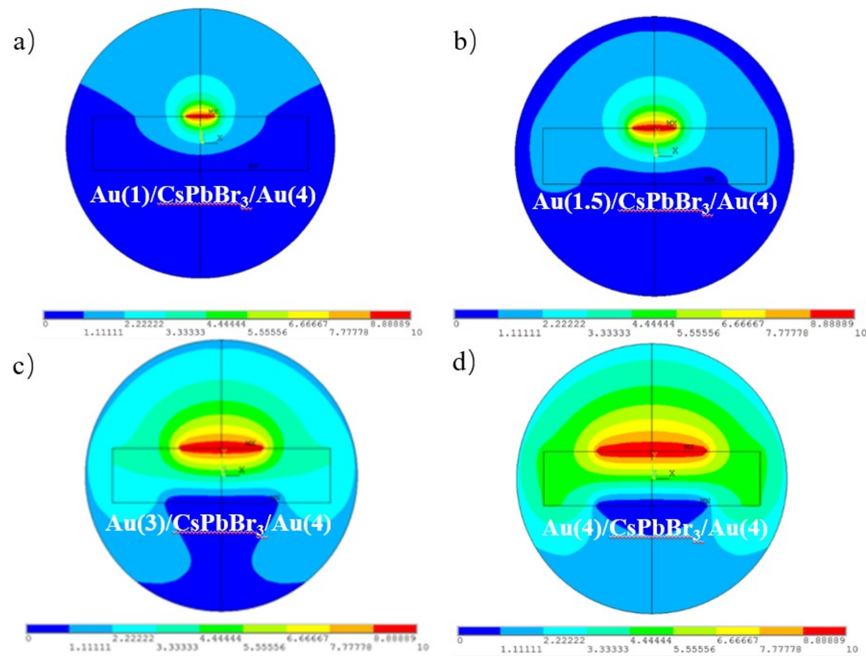


**Figure S4.** Electric-field intensity-distribution cloud maps: a) Au(1)/$CsPbBr_3$/Au(4); b) Au(1.5)/$CsPbBr_3$/Au(4); c) Au(3)/$CsPbBr_3$/Au(4); d)Au(4)/$CsPbBr_3$/Au(4).

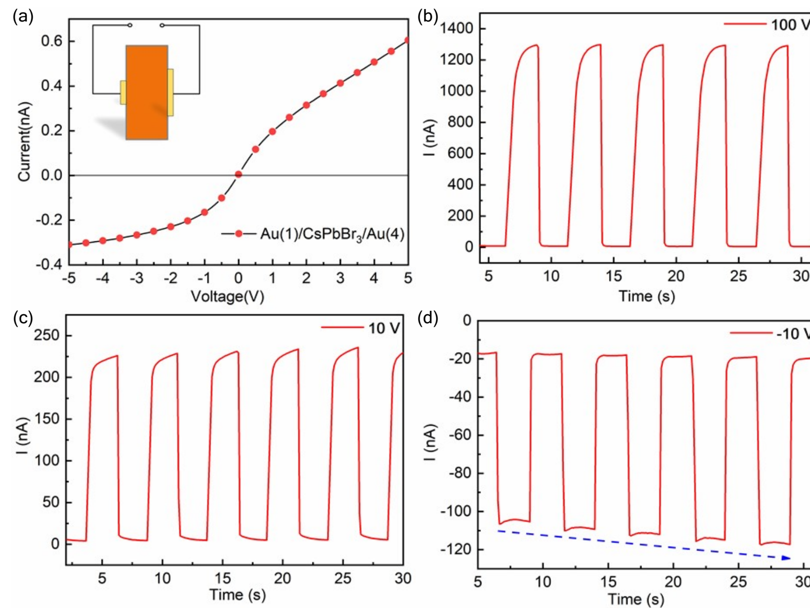


**Figure S5.** (a) I-V characteristics, and light response of Au(1)/$CsPbBr_3$/Au(4) device at (b)100 V, (c)10 V and (d)-10 V, respectively.

Figure S5 (a) shows that a potential barrier is generated for Au(1)/$CsPbBr_3$/Au(4) device. When the forward voltage applied to the device is 100 V, as shown in Figure S5 (b), it can be seen from the photocurrent response that the device still has good stability. Figure S5 (c) and S5 (d) show the photoresponse characteristics of the Au(1)/$CsPbBr_3$/Au(4) device under pulsed light at different bias voltage. The photocurrent at 10 V and -10 V bias voltage are 300 nA and 25 nA, respectively. The leakage current at the applied reverse voltage is one order of magnitude smaller than that under forward voltage. However, the reverse response is unstable and the photocurrent is small. Therefore, a forward voltage is applied to the device to test its characteristics.

**Table S3.** The switching signal-to-noise ratio of devices with different electrode diameter ratio under 365 nm periodic light.

| electrode diameter ratio | 1 mm:4 mm | 1.5 mm:4 mm | 3 mm:4 mm | 4 mm:4 mm |
|---|---|---|---|---|
| signal-to-noise ratio | 200 | 180 | 28 | 17 |

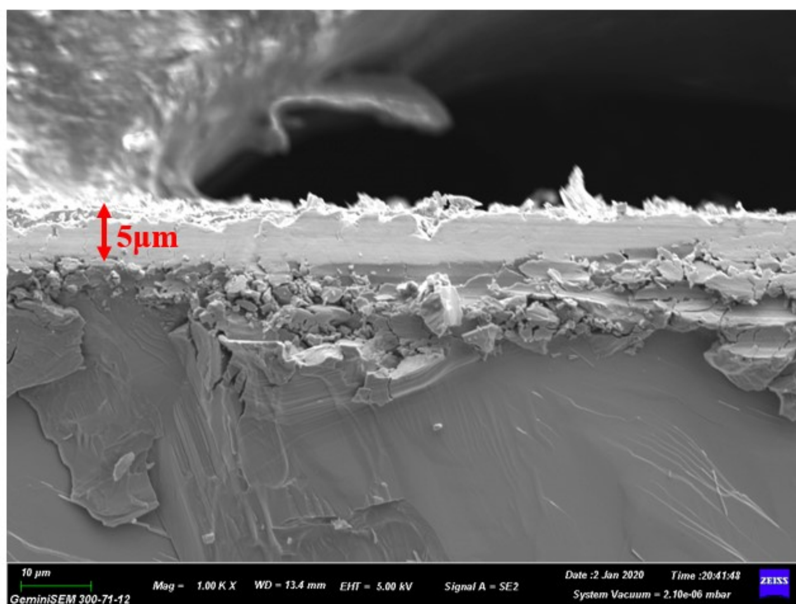


**Figure S6.** For the Au(4)/CuI/$CsPbBr_3$/Au(4) device, the thickness of CuI was nearly 5 um.

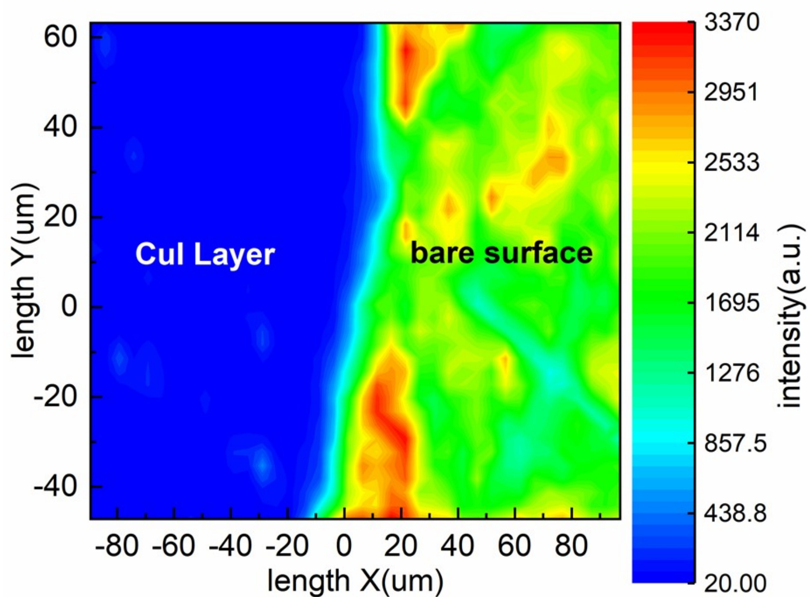


**Figure S7.** PL mapping for the surface of $CsPbBr_3$ wafer

In order to distinguish PL intensity between CuI layer and the surface of bare wafer, we only coated CuI on half part of the wafer surface and took the profile. The intensity of PL greatly quench after introducing the CuI layer.

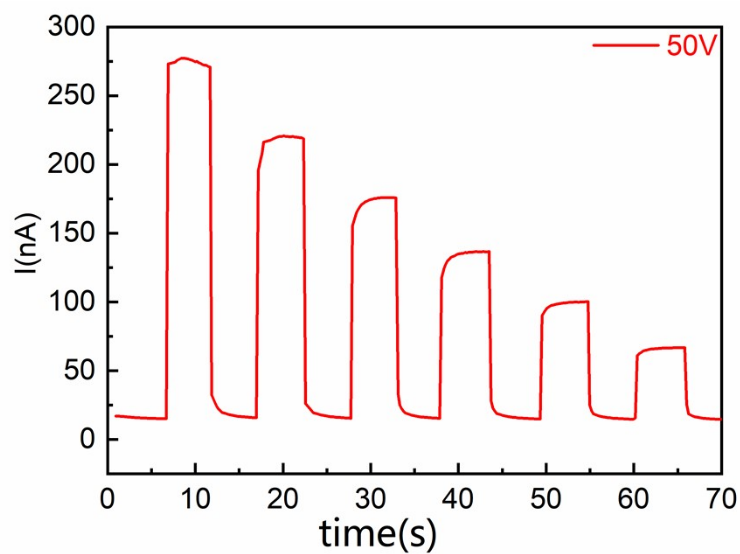


**Figure S8.** For the Au(4)/CuI/$CsPbBr_3$/Au(4) device, after stored in air for 6 months, the leakage current of the detector increased slightly to 16 nA under a bias of 50 V.